Tethered Small-Molecule Acceptors Simultaneously Enhances the Efficiency and Stability of Polymer Solar Cells

Shangyu Li [a, #], Rui Zhang [b, #], Ming Zhang [a, #], Jia Yao [a], Zhengxing Peng [c], Qi Chen [a], Cen Zhang [a], Bowen Chang [a], Yang Bai [a], Hongyuan Fu [a], Yanni Ouyang [d], Chunfeng Zhang [d], Julian A. Steele [e, f], Thamraa Alshahrani [g], Maarten B.J. Roeffaers [e], Eduardo Solano [h], Lei Meng [i], Feng Gao *[b], Yongfang Li [i], and Zhi-Guo Zhang [a, *]

[a] State Key Laboratory of Organic/Inorganic Composites, Beijing Advanced Innovation Center for Soft Matter Science and Engineering, Beijing University of Chemical Technology, Beijing 100029, China

[b] Department of Physics, Biomolecular and organic electronics, Chemistry and Biology (IFM), Linköping University, Linköping, SE-58183, Sweden

[c] Advanced Light Source, Lawrence Berkeley National Laboratory, Berkeley, CA 94720, United States

[d] National Laboratory of Solid State Microstructures, School of Physics, and Collaborative Innovation Center for Advanced Microstructures, Nanjing University, Nanjing, 210093, P. R. China

[e] cMACS, Department of Microbial and Molecular Systems, KU Leuven, Celestijnenlaan 200F, 3001 Leuven, Belgium

[f] School of Mathematics and Physics, The University of Queensland, Brisbane, QLD, 4072, Australia

[g] Department of Physics, College of Science, Princess Nourah bint Abdulrahman University, Riyadh, 11671, Saudi Arabia

[h] NCD-SWEET beamline, ALBA Synchrotron Light Source, 08290 Cerdanyola del Vallès, Spain

[i] Beijing National Laboratory for Molecular Sciences, CAS Key Laboratory of Organic Solids, Institute of Chemistry, Chinese Academy of Sciences, Beijing 100190, China

E-mail: feng.gao@liu.se (F. Gao), zgzhangwhu@iccas.ac.cn (Z.G. Zhang)

Abstract

Polymer solar cells (PSCs) have seen rapid progress in recent years, whereby the mixture of polymer donors and small-molecule acceptors (SMAs) are fine-tuned to realize a favorable kinetically trapped morphology and thus a commercially viable device efficiency. However, the thermodynamic relaxation of the mixed domains within the blend raises concerns related to the long-term operational stability of the devices, especially in the record-holding A-DA'D-A type SMAs (typically identified

as Y6). In addressing this challenge, we report a new class of dimeric Y6-based SMAs tethered with differential flexible spacers to regulate their aggregation and relaxation behavior. In their polymer blends with PM6, we find that they favor an improved structural order relative to that of Y6 counterpart as evidenced by their shorter facial π-π stacking distance and larger crystal coherence length, leading to higher and more balanced charge transport in device. Most importantly, with flexible spacers to restrict the motion of individual SMAs, the tethered SMAs show large glass transition temperatures to suppress the thermodynamic relaxation in mixed domains, which is also evidenced by the larger Flory–Huggins interaction parameter with the polymer donor. For the high performing dimeric blend, an unprecedented open circuit voltage of 0.87 V is realized with a conversion efficiency of 17.85%, while those of regular Y6-base devices only reach 0.84V and 16.9%, respectively. Most importantly, the dimer-based device possess substantially reduced burn-in efficiency loss, retaining more than 80% of the initial efficiency after operating at the maximum power point under continuous illumination for 700 hours. Our tethering approach provides a new direction to simultaneously develop PSCs with high efficiency and excellent operating stability.

Kew words: Tethered small-molecule acceptor, Thermodynamically stable, Device stability, Organic solar cells

Introduction

Solution-processable polymer solar cells (PSCs) have attracted immense attention due to their advantageous ability to print flexible, lightweight, and large area devices, via roll-to-roll processes.[1-2] The last five years have witnessed the promising development of non-fullerene small-molecule acceptors (SMAs) [2-4] with strong optical absorption and tunable molecular structures, yielding power conversion efficiency (PCE) of 18-19%.[5-15] As their PCEs get closer to the requirements for commercial viability, focus must critically shift toward the challenges associated with their long-term operational stability.[16-20]

In PSCs, a bulk-heterojunction (BHJ) structure is required to facilitate exciton dissociation and carrier collection, in which the blending of the polymer donor and SMAs are kinetically trapped to produce a fine-mixed domains.[21-22] Such deliberately tuned BHJ morphology maximize the device PCE and, specifically for the case of record-holding PSCs based on Y-series SMAs (such as Y6), [23-

[25] the BHJ is also the source of burn-in degradation throughout the device lifetime. This is because the thermodynamic relaxation of the mixed domains within the blend is unavoidable, i.e. from their initial trapped state to the bimodal state, which mediates the degradation process over time, especially at elevated temperatures.[26-30] Recent studies have discovered that suppressing the demixing and crystallization of the SMAs with low diffusion coefficients in the blend can help achieve long-term stability of PSCs.[31] To suppress the diffusion of the SMAs, their results further highlight the importance of their high glass transition temperature (T_g) for a high activation energy on diffusion.[31]

Notably, all-polymer solar cells (*all*-PSCs) with the polymer acceptor, which typically has lower diffusivity than small molecules, represent an alternative route to develop stable PSCs.[32-34] Recently, polymerized SMAs (PSMAs) have greatly advanced the performance of *all*-PSCs; however their efficiency is still inferior to their SMA-based counterparts.[35] To fill the efficiency gap, further investigations are required,[36-38] such as new polymerization methods of PSMAs to avoid device performance dependence on the molecular weight, and new conjugated linkages to promote polymer interchain stacking. Inspired by the inherent high stability of PSMAs, the use of two or three conjugated segments of PSMAs, to develop SMA-based oligomers characterized with a strictly uniform molecular structure, offers a promising strategy.[39-42] However, the construction of such molecular fragments usually has a low yield (typical 30-40 %) due to the difficulty in the synthesis of the key intermediate (monobrominated SMA), which ultimately increases their production cost. A heavy reliance on toxic tin compounds and noble metal catalysts to couple the SMA units also causes environmental concerns within a commercial setting.

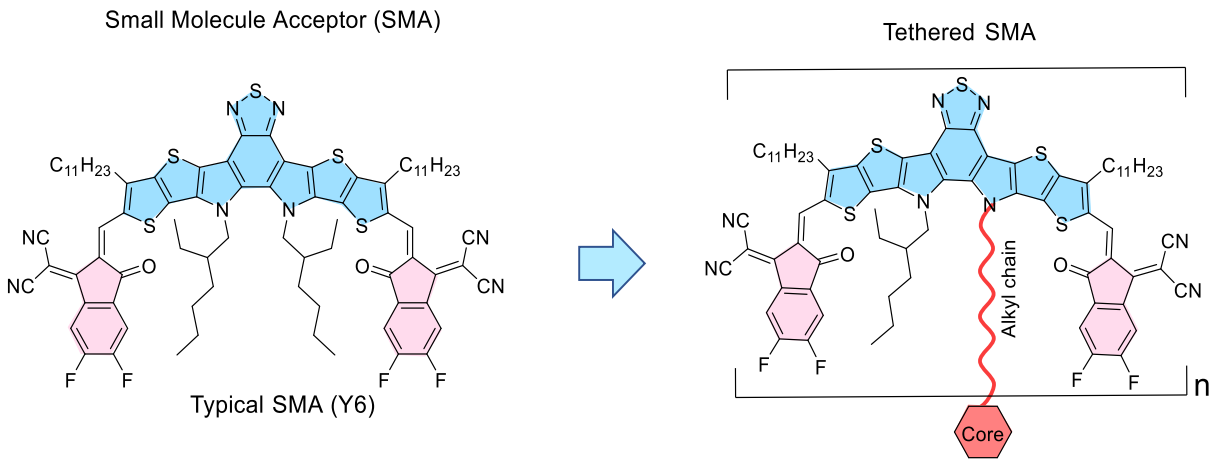

Figure 1. Design concept on tethered SMAs, where *n* represents the number of the SMAs attached

to the core.

To address these challenges, we propose here an alternative approach of covalently tethering SMAs via an environmentally friendly and effective synthesis of dimeric acceptors (design concept provided in Figure 1). For the dimeric fragments, under a conventional nucleophilic reaction, the Y6-derived SMAs are easily linked to a benzyl core via a flexible spacer. Also, it has been well established that the electronic states coupling of the SMAs significantly affect the exciton splitting in devices [43]; thus in the dimers (Figure 2), the distance of individual SMAs can be gradually tuned to manipulate their molecular packing, resulting in **DY1** with a hexyl space (n = 1), **DY2** with an octyl spacer (n = 2), and **DY3** with a decyl spacer (n = 3) attached on the benzyl core. Subsequently, the volume of the molecular size is increased with the SMAs being tethered together, which is suggested to reduce their diffusivity in the polymer blend due to a restriction in available molecular motion.[31] Through our approach we can completely change the molecular aggregation behavior relative to their individual SMA counterpart, leading to dramatically increased efficiency and stability in devices.

Results and discussions

Materials Synthesis and Characterization

Our synthesis route for realizing tethered dimeric SMAs is illustrated in Figure 2a. Starting with the commercially available precursor **1**, the dimeric key skeleton **2** was obtained in a one-pot nucleophilic reaction by sequential addition of different alkyl bromides. Followed by a Vilsmeier-Haack reaction using dry *N*, *N*-dimethylformamide (DMF) and $POCl_3$, aldehyde-based compound **3** was obtained. Notably, the desired dimers can be nearly quantitatively obtained via our newly developed $BF_3{\cdot}OEt_2$-catalyzed Knoevenagel condensation [44] from compound **3**. With the flexible alkyl side chains to tether the SMAs, it can bring excellent solubility in organic solvents for device processing, which is different from the aromatic linkers in PSMAs and SMAs.

While in a dilute solution, the UV–visible absorption spectra of the dimers (Figure 2b and 2c) are slightly redshifted relative to that of Y6. This mainly comes from forcing a closer distance between individual SMAs in one dimer molecule, which is nearer than that of neighboring Y6 units in the dilute solution. Interestingly, the absorption spectra of the dimer-based films become broader (Figure

2c), and their absorption peaks are also blue-shift by ca. 30 nm compared to Y6 film. This phenomenon suggests that the linkers of the dimers could inhibit their initial packing behavior in the as-cast films, which is further supported by the gradual red-shift of the maximum absorption peak from **DY1** to **DY2**, and **DY3**. This is because a gradually increased linker will provide more freedom for packing of the tethered Y6 molecule in film. In the dimers, the distinct intermolecular and intramolecular interactions represent valuable parameters for controlling thin-film crystallization and morphology when blended with donors in PSCs, which will be discussed further in the following section.

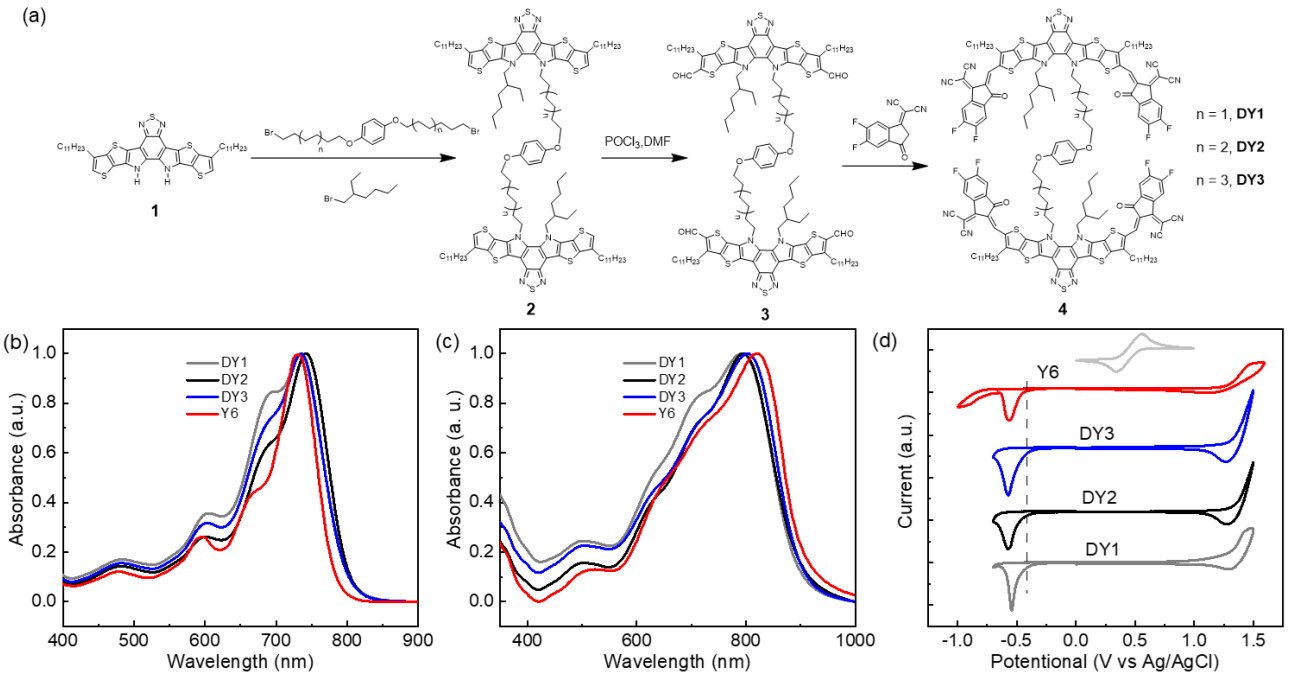

Figure 2. (a) Synthetic routes of the dimers. Normalized UV-vis absorption spectra of the SMAs in (b) dilute solution and (c) as-cast film. (d) Cyclic voltammograms of the SMAs.

The electronic energy levels of the dimers and Y6 were measured by cyclic voltammetry (Figure 2d). The dimers exhibit similar lowest unoccupied molecular orbital (LUMO) energy levels with each other, the values are slightly upshift relative to Y6, which may provide a larger open circuit voltage (V_{OC}) in devices. With increasing linker length, we can expect that it becomes easier for the dimers to break the entanglements for a better molecular motion. From the differential scanning calorimetry (DSC) measurements (Figure 3a), they exhibit decreased melt points of 321.7 °C for **DY1**, 302.5 °C for **DY2**, and 279.8°C for **DY3**, for which their progressively decreased melting enthalpy (ΔH_m) are

27.0, 24.6, and 13.3 J g^{-1}, respectively.

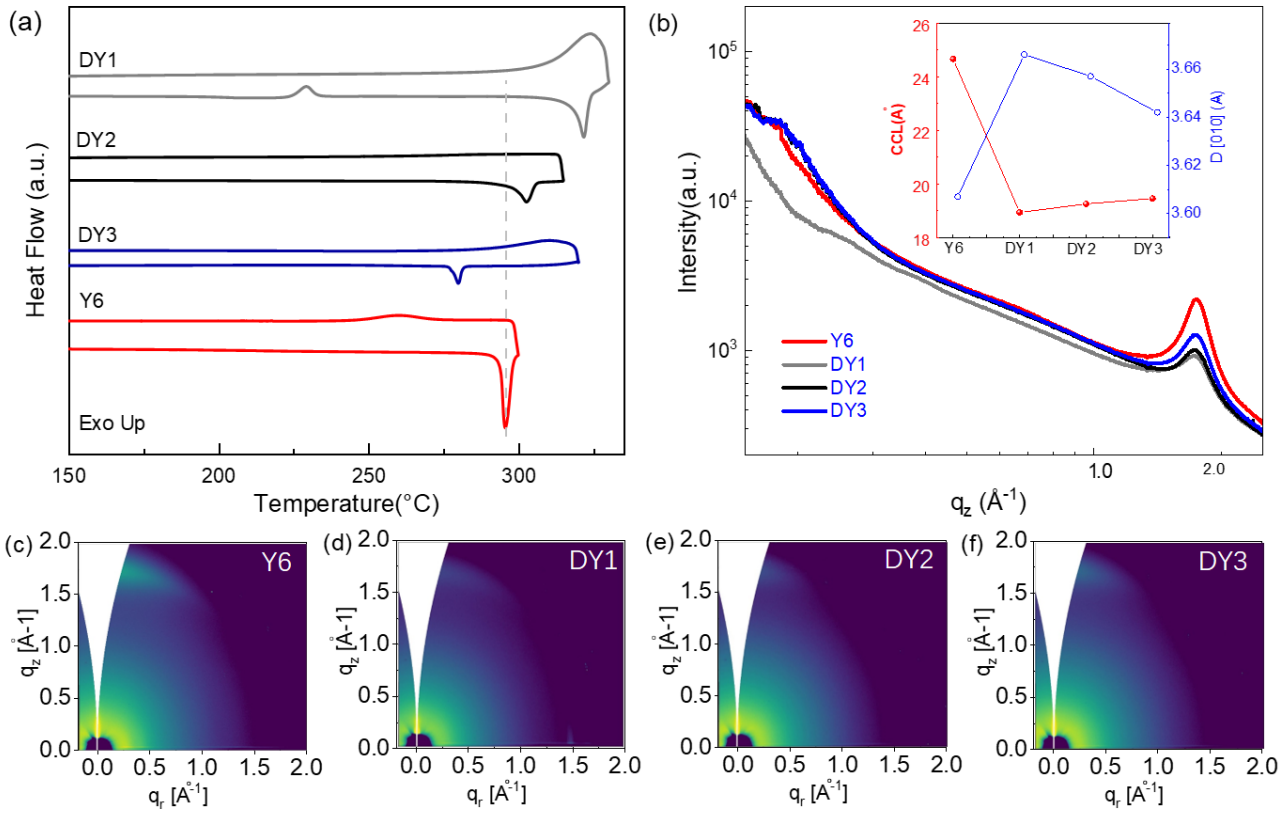

Figure 3. (a) DSC thermograms of Y6 and the dimers with a higher heating rate of 10 °C min^{-1} under nitrogen atmosphere. (b) Line cuts of the GIWAXS images with the integrated azimuthal angle range from 80° to 100°, the inset shows the π-π stacking distance versus the CCL lengths of the SMAs. The GIWAXS diffraction patterns of as-cast films: (c) **Y6**, (d) **DY1**, (e) **DY2**, (f) **DY3**.

The glass transition temperature (T_g) is a critical thermal property of organic photovoltaic materials that can be used to guide the morphology control and predict morphological stability. In general, the T_g values of SMAs are connected to their diffusion and crystallization in the active layer. Since all the three dimers and Y6 materials exhibit no glass transition signals in the DSC scan, we estimate their T_g values with absorption spectroscopy following the method provided by Ade and co-authors.[30] All the dimers possess higher T_g values (>122°C) compared to Y6 (101 °C), which can suppress the diffusion-enabled demixing in their polymer blend for better device stability. For the dimers, with increasing spacer size, their T_g values decrease (Figure S1), i.e. 127 °C for **DY1**, 122 °C for **DY2** and 115 °C for **DY3**, suggesting easier thermal relaxation of the molecular structure with a longer spacer.

To understand why dimerization can affect the molecular packing, we probed the microstructures with two-dimensional grazing-incidence wide angle X-ray scattering (2D GIWAXS). As shown in Figure 3b, with the linker gradually changed from hexyl group to octyl group, and decyl group on the benzyl core, the π-π stacking distance ($d_{\pi-\pi}$) in the out-of-plane (OOP) direction showed an increased trend compared with Y6 (3.61 Å), although just slightly difference appeared. The results show that although the linkers increase the spatial distance, they make weak influence on the molecular packing. Accordingly, the crystalline coherence length (CCL) showed slightly decreased crystallinity sizes (Figure 3b) in tethered SMAs compared with Y6, which also represent weak influences of the linkers on the relative micro-scaled sizes in the neat films. All the fitting results suggests that tethered dimers can be used as a general strategy to afford small molecule clusters without influence on the nano- and micro-scaled morphologies.

Table 1. Comparison of the crystallinity, thermal and physicochemical properties of the acceptors.

Acceptors	λ_{max} (nm) [a]	λ_{max} (nm) [b]	d [010] (Å) [c]	CCL[010] (Å)	T_m (°C)	ΔH_m (J g^{-1})	T_g (°C) [d]	E_g^{opt} (eV) [e]	E_{LUMO} (eV)[f]	E_{HOMO} (eV)[f]
Y6	730	820	3.61	24.70	295.6	28.3	90.5	1.369	-3.90	-5.65
DY1	742	790	3.67	18.94	321.7	27.0	127.4	1.390	-3.93	-5.70
DY2	734	794	3.66	19.26	302.5	24.6	122.7	1.379	-3.95	-5.75
DY3	733	802	3.64	19.46	279.8	13.3	115.4	1.376	-3.95	-5.72

[a] Solution; [b] Film; [c] Calculated from Scherer equation: CCL = 2πK/Δq, where Δq is the full-with at half-maximum of the peak and K is a shape factor (0.9 was used here); [d] Estimated with absorption spectroscopy [e] Calculated from the absorption edge of the films: $E_g^{opt} = 1240/\lambda_{edge}$. [f] Calculated according to the equation: $E_{LUMO/HOMO} = -e\,(E_{red/ox} + 4.36)$ (eV).

Photovoltaic Properties

To evaluate the effect of the dimerization on device performance, we fabricated conventional devices with a structure of indium tin oxide (ITO)/PEDOT: PSS (poly (3,4-ethylenedioxythiophene): poly(styrene-sulfonate))/PM6: acceptors (w/w, 1: 1.2)/PDINN (aliphatic amine-functionalized perylene-diimide)/ Ag cathode. The devices were optimized under a kinetically trapped method with annealing time of 100 °C to promote the aggregation of the SMAs and their phase separation with PM6. Compared with Y6 which requires an annealing time of 10 min, an extended time of 30 min is needed for all the dimers, which may be associate with their lower diffusion coefficients as revealed

by their high T_g values.[31] In general, high diffusion coefficients of the SMAs can lead to a higher nucleation density of crystals, faster crystal growth and lower stability in device, which will be discussed below.

Table 2. Photovoltaic parameters of the devices based on PM6: acceptors with D/A weight ratio of 1: 1.2 and thermal annealing under the illumination of AM1.5G, 100 mW/cm^2.[a]

Acceptor	V_{oc} [V]	J_{sc} [mA•cm^{-2}]	FF [%]	PCE [%]	μ_h [10^{-4}cm^{2}v^{-1}s^{-1}]	μ_e [10^{-4}cm^{2}v^{-1}s^{-1}]	μ_h/μ_e
Y6	0.84	26.32	76.17	16.93 (16.42 ± 0.51)	3.10	2.24	1.38
DY1	0.87	25.67	73.24	16.46 (15.95 ± 0.51)	3.94	2.74	1.44
DY2	0.87	26.60	76.85	17.85 (17.33± 0.52)	4.41	3.29	1.34
DY3	0.87	26.20	76.21	17.33 (16.87 ± 0.46)	3.87	2.77	1.40

[a] Average values based on ten devices.

PSCs fabricated using Y6 delivered a PCE of 16.93% along with J_{sc} of 26.32 mA/cm^2, FF of 76.17% and V_{OC} of 0.84 V. For the dimer-based devices, one obvious advantage is their significantly high V_{OC} of ca. 0.87 V. Compared with Y6, the slight blue shift of the film absorption may partially contribute to the V_{OC} increase. In order to understand how the tether strategy of the SMAs affect the V_{OC} in the devices, we measured the energy losses of the photovoltaic devices by characterizing Fourier-transform photocurrent spectroscopy (FTPS-EQE) and electroluminescence (EL) spectra in their corresponding PSCs. The total energy loss (ΔE) can be quantified via detailed balance theory, and is split into three contributions ($\Delta E = \Delta E1 + \Delta E2 + \Delta E3$): Here $\Delta E1$ represents the unavoidable radiative recombination loss above the bandgap (E_g), $\Delta E2$ denotes the radiative recombination loss below the E_g, and $\Delta E3$ captures the nonradiative energy loss.[45] The values for E_g were calculated from the derivatives of the EQE curves using the following equation: $E_g^{PV} = \frac{\int_a^b E_g \cdot P(E_g) \cdot dE_g}{\int_a^b P(E_g) \cdot dE_g}$, where E_g^{PV} is the photovoltaic band gap energy in the blends.[46] The E_g values of the two devices were calculated to be 1.41 eV and 1.43 eV for PM6/Y6 and PM6/**DY2**, respectively (Figure S2). From the calculation, both blends exhibited similar $\Delta E1$ values (0.26 eV for PM6/Y6 and 0.27 eV for PM6/**DY2**), while the devices based on Y6 and **DY2** also displayed a consistent sharp band edge in their highly sensitive EQE spectra, resulting in similar $\Delta E2$ values (0.05 eV, 0.06 eV; Figure S3). In

addition, the electroluminescence quantum efficiency (EQE_{EL}) of these two blends were also similar, resulting in $\Delta E3$ values of 0.26 eV for PM6/**DY2** and 0.27 eV for PM6/Y6 (Table S1). Therefore, as expected, the V_{OC} increase mainly results from an increase in the bandgap energy, and the energy losses are similar. In other words, our tethered dimer strategy by using flexible chains has almost no influence on the energy loss in the solar cell while increasing the intrinsic thermodynamic stability of the materials and device. For the dimers, **DY1** delivered a PCE of 16.46% with J_{sc} of 25.67 mA/cm^2, FF of 73.24% along with a V_{OC} of 0.87V. When the chain length is increased, **DY2** yielded a significantly increased FF of 76.85%, thus a higher PCE of 17.85%. Further increasing the spacer slightly decreases the efficiency, resulting in 17.33% for **DY3**.

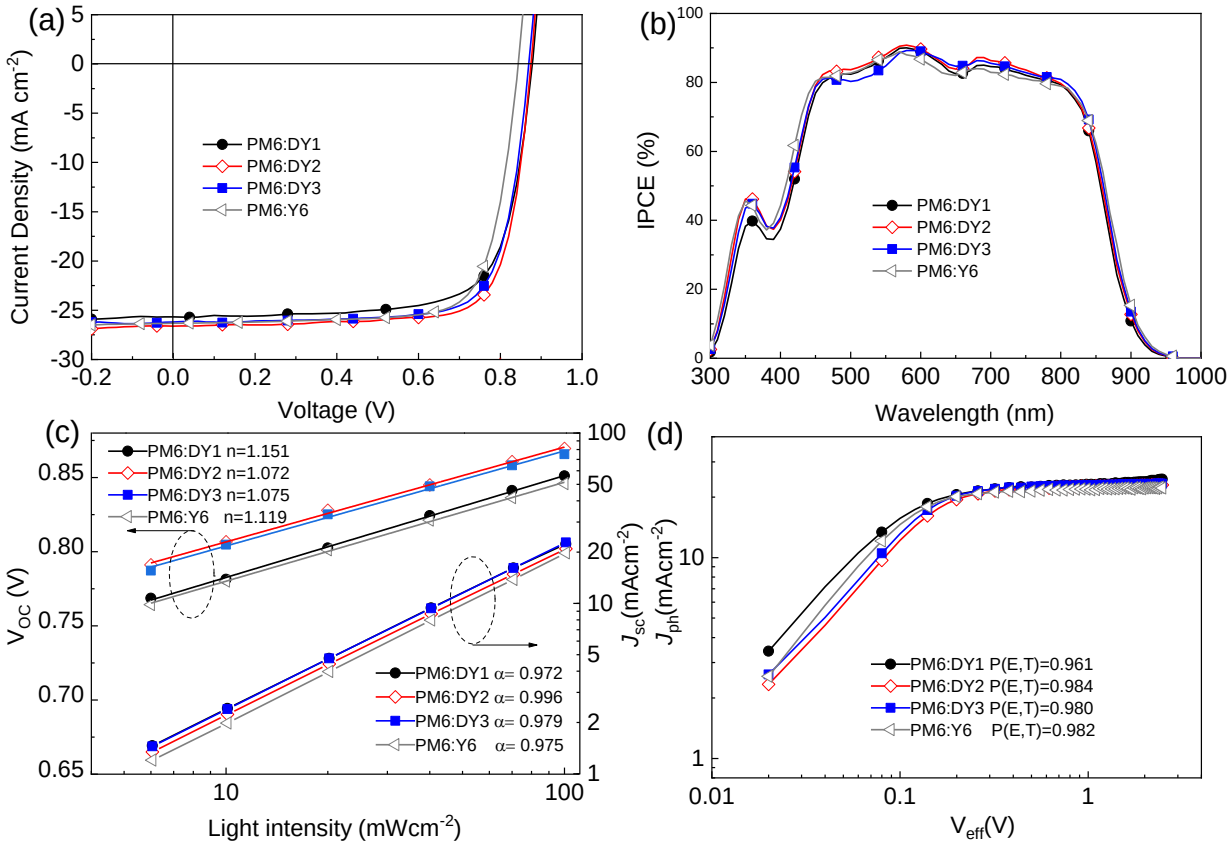

Figure 4. (a) *J*-V curves of the best PSCs (w/w, 1: 1.2) under the illumination of AM 1.5G, 100 mW cm^{-2} and (b) IPCE spectra of corresponding PSCs. (c) Light intensity dependence of J_{sc} and V_{OC} of the PSCs. (d) J_{ph} versus V_{eff} of the optimized devices.

Along with a broad photo response from 300 to 900 nm, the maximum incident photon to converted current efficiency (IPCE) values (Figure 4b) are all over 88%, indicating efficient photon harvesting

and charge collection in active layers. The J_{SC} values calculated from the IPCE spectra were 25.55 mA/cm^2, 25.17 mA/cm^2, 25.70 mA/cm^2 and 25.56 mA/cm^2 for Y6, **DY1**, **DY2** and **DY3**-basd device respectively, which are in good agreement with the J_{SC} value obtained from the *J*-V curves within a 5% mismatch.

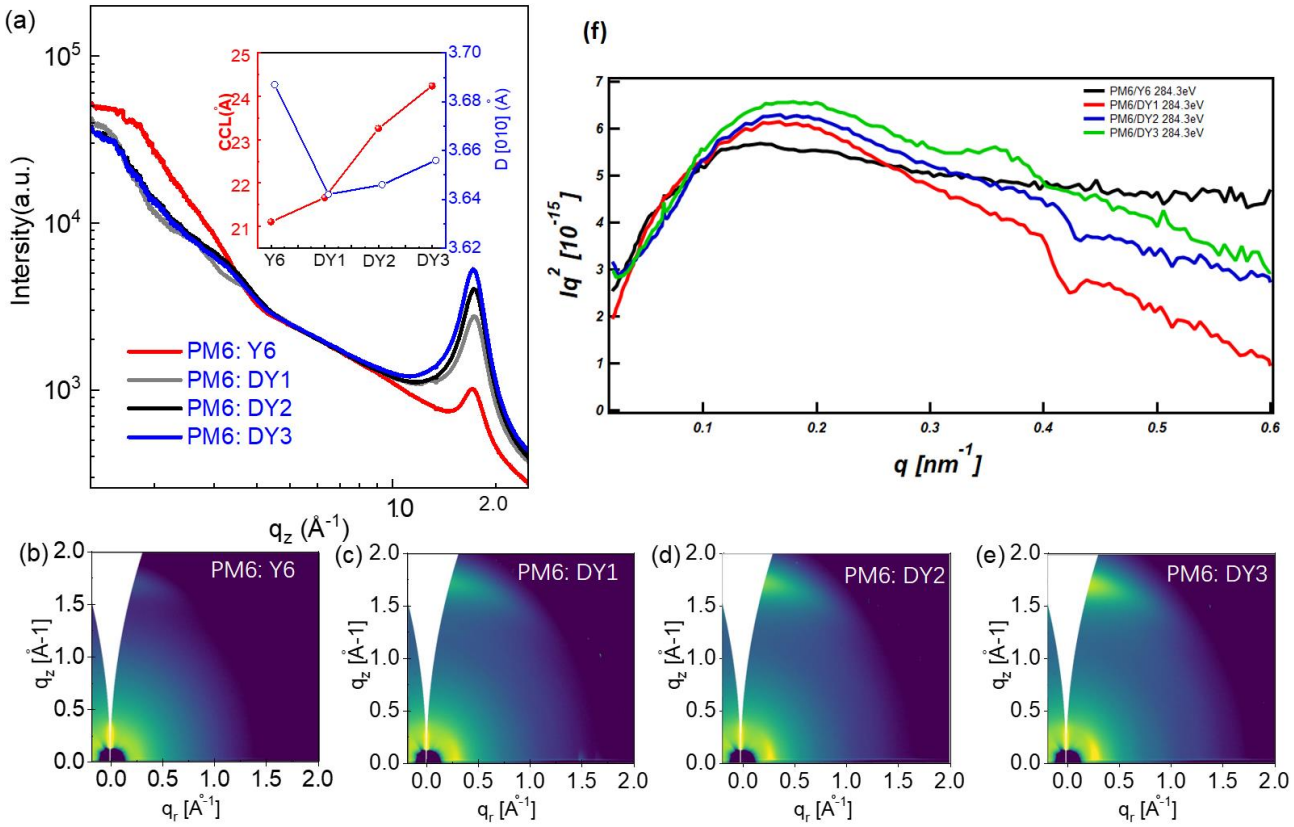

Figure 5. (a) Line cuts of the GIWAXS images with the integrated azimuthal angle range from 80° to 100°, the inset shows the π-π stacking distances along with the CCL lengths. The GIWAXS diffraction patterns of annealed blend films: (b) PM6: **Y6**, (c) PM6: **DY1**, (d) PM6: **DY2** and (e) PM6: **DY3**. (f) RSoXS profiles under 284.3eV for PM6/Y6, PM6/DY1, PM6/DY2, PM6/DY3, respectively.

Further examination of the dimer-based blends, we find that they favor a shorter $d_{\pi\text{-}\pi}$ distance, relative to that of Y6-based blend (Figure 5). Notably, compared with the pristine films, the $d_{\pi\text{-}\pi}$-stacking distance of the dimers is slightly decreased (inset of Figure 5a), which might result from the restriction of the conjugated polymer donor in the dimer-based blend. In parallel, their CCL values of the dimers is larger than that of Y6, and gradually increased when the linker length increased (21.66 Å for **DY1**-based blend, 23.26 Å for **DY2**-based blend, 24.24 Å for **DY3**-based blend). Compared to Y6-based blend, the shorter $d_{\pi\text{-}\pi}$-stacking distance and the larger domain size (discussed below) in the

dimer-based blends may contributed to an increased CCL value. The relative degree of crystallinity (rDOC) was calculated to quantitatively compare the crystallinity degree.[47-48] The obtained rDOC values of the π-π stacking are 0.90, 0.91, 0.95, 1.00 for PM6/Y6, PM6/**DY1**, PM6/**DY2**, PM6/**DY3**, respectively, which shows relative higher crystallinity degree in tethered systems. In addition, we integrated distribution of the (010) diffraction peak under different azimuthal angles (Figure S4), the relative face-on/edge-on orientation ratios are 0.94, 1.00, 0.99, 0.98 for PM6/Y6, PM6/**DY1**, PM6/**DY2** and PM6/**DY3**, respectively, suggesting a preferred face-on orientation formed in tethered SMAs based blend systems compared with Y6 based blends.[49] In general, strong face-on orientation and the shorter π-π stacking distances are desirable for higher charge carrier mobility thereby efficiencies.

Then, the relative domain sizes and domain purities in micro-scaled size are discussed quantitatively by using resonant soft X-ray scattering (RSoXS) (Figure 5f and Table S2). From the RSoXS profiles, the corresponding long period of phase separation (relating to the center-to-center domain spacing) can be estimated from peak positions. All the long period *q* peaks for tethered-based systems show an obvious increasement compared with Y6-based blend (0.138 nm^{-1} for PM6/Y6, 0.138 nm^{-1} for PM6/**DY1**, 0.165 nm^{-1} for PM6/**DY2**, 0.175 nm^{-1} for PM6/**DY3**), which represents the decreasing of long period from 45.35 nm (PM6/**Y6**, PM6/**DY1**), to 38.00 nm (PM6/**DY2**), and 35.90 nm (PM6/**DY3**), respectively. In addition, the average domain sizes (calculated by using Scherrer equation) are increased in PM6/**DY1** (28.59 nm) and PM6/**DY2** (26.62 nm) compared with PM6/Y6 (22.32 nm), which can improve the exciton diffusion in devices. The relative integrated scattering intensity (ISI) is proportional to the root-mean-square composition variations, which are monotonically related to the average phase purity. The relative purity of PM6/Y6, PM6/**DY1**, PM6/**DY2**, PM6/**DY3** are calculated to be 0.86, 0.81, 0.99, 1.00, respectively. What we should mention here is that although PM6/**DY3** shows the highest domain purity, but the decreased average domain size limits the further increasement of the short current, which accounts well with the evolution of the device parameters.

The charge carrier mobilities of the active layers were estimated using the space charge limited current (SCLC) method, and the results are shown in Table 2. For the Y6 based device, their hole (μ_h) /electron (μ_e) mobilities are estimated to be 3.10×10^{-4} $cm^2V^{-1}s^{-1}$/$2.24\times10^{-4}cm^2V^{-1}s^{-1}$ with μ_h/μ_e of

1.38, whereas for the dimers-based devices, their corresponding hole/electron mobilities are both increased: 3.97×10^{-4} $cm^2V^{-1}s^{-1}$/$2.74\times10^{-4}cm^2V^{-1}s^{-1}$ with μ_h/μ_e of 1.44 for **DY1**, 4.41×10^{-4} $cm^2V^{-1}s^{-1}$/$3.29\times10^{-4}cm^2V^{-1}s^{-1}$ with μ_h/μ_e of 1.34 for **DY2**, 3.87×10^{-4} $cm^2V^{-1}s^{-1}$/$2.77\times10^{-4}cm^2V^{-1}s^{-1}$ with μ_h/μ_e of 1.40 for **DY3**. The high and more-balanced hole/electron mobilities for the **DY2**- and **DY3**-based blend films are beneficial for improving the device performance.

The role of spacer length in dimers

The charge carrier recombination behavior of the PSCs was further investigated by the dependence of J_{sc} and V_{oc} on the light intensity (P).[50] The J_{sc} (and V_{oc}) versus P is shown in Figure 4c. The typical relationship between J_{sc} and P is expressed as $J_{sc} \propto P^{\alpha}$.[51-52] The value of α here should be equal to 1 if all of the free carriers were extracted by the electrode.[50] It can be seen from Figure 4c, the α values for the **DY1**-based device, **DY2**-based device, **DY3**-based device, Y6-based device are 0.972, 0.996, 0.979, and 0.975, respectively. This means that there is effective carrier collection and negligible bimolecular recombination in the best-performing **DY2**-based devices at the short-circuit condition. Figure 4c also shows the dependence of V_{OC} on the natural logarithm of light intensity (ln$P$), the slopes of which are 1.151 kT/q for **DY1**, 1.072 kT/q for **DY2**, 1.075 kT/q for **DY3** and 1.119 kT/q for Y6. The slopes of the **DY2** and **DY3**-based devices approach kT/q, indicating dominant bimolecular recombination at the open-circuit condition.[50]

To gain insights on exciton dissociation and charge collection behavior of the PSCs, the charge dissociation probability ($P(E,T)$) was estimated via its relationship to the photo current density (J_{ph}) and the effective voltage (V_{eff}) of the dimer-based devices. The photocurrent density J_{ph} is defined as $J_{ph} = J_L - J_D$, where J_L and J_D are the photocurrent densities under AM 1. 5G illumination and in the dark condition, respectively. The effective voltage V_{eff} is defined as $V_{eff} = V_0 - V_{bias}$, where V_0 is the voltage at which J_{ph} is zero and V_{bias} is the applied external voltage bias. It can be seen from Figure 4d that, the increase in V_{eff} results a higher internal electric field in the device and, accordingly, the charge recombination will be minimized. In our cases, J_{ph} tends toward an approximate saturation value (J_{sat}) at a sufficiently high V_{eff} of 2.0 V. Thus, it follows that the charge dissociation probability ($P(E,T)$) can be estimated from equation of $P(E,T) = J_{ph}/J_{sat}$. Under the short-circuit conditions, the **DY2** and **DY3**-based devices have $P(E,T)$ values over 0.980, which are both higher than the **DY1**-based device (0.961). This indicates, when designing the dimers, a suitable length for the spacer is

necessary to increase exciton dissociation in the device. The results collectively suggest that a suitable spacer is important to reduce the bimolecular recombination and increase exciton dissociation in device when design dimers, and an octyl group (such as in **DY2**) is good choice as a spacer for tethered dimers.

The effect of dimerization on device stability

As the **DY2**-based device performs best in efficiency, we compare its device stability with Y6-based device. Initially, device stability was tested at a maximum power point (MPP) under white light for glass encapsulated devices in air, with the normalized PCEs shown in **Figure 6a**. The PCEs of Y6-based device decrease over 50% after operating for 80 h, a response of which is typical of light induced burn-in losses.[16] The trend of device degradation is consistent with previous report.[53] In contrast, the **DY2**-based devices show substantially less burn-in efficiency loss on this timescale, and exhibit a PCE loss of 17% after 700 h. Furthermore, thermal stress was applied for unencapsulated devices under dark in nitrogen-filled glovebox. As shown in **Figure 6b**, the **DY2**-based device shows a negligible PCE loss after 480 h, while that of the Y6-based device dropped by 40% after 120 h.

Previous work has confirmed that phase separation, and thus the morphological stability, is strongly dependent on the diffusion coefficients of the SMAs which can be predicted by their T_gs values.[31] To further confirm this concept, we measured the RSoXS for the PM6/Y6 and PM6/**DY2** blend before and after thermal annealing processed (Figure S5). From the results, we could find the long period in PM6/Y6 decreased from 45.47 nm to 38.67 nm, while 38.00 nm to 36.79 nm in PM6/**DY2** blends when annealing for 3 hours. Furthermore, the average domain sizes in PM6/Y6 decrease from 22.32 nm to 9.07 nm, while 26.62 nm to 22.55 nm in PM6/DY2 blends respectively. The relative purities are 1 for PM6/Y6 (thermal annealed 3 hours at 110 °C) and 0.42 for PM6/**DY2** (thermal annealed 3 hours at 110 °C), which suggests that Y6 molecules moved obviously in the bulk heterojunction blends above the T_g. Both long period and average domain sizes show an obvious increased stability in PM6/**DY2** blends under thermal annealing. As mentioned above, the dimers favor a significantly high glass transition relative to that of Y6, and therefore provide a higher activation energy toward diffusion in their polymer blend.

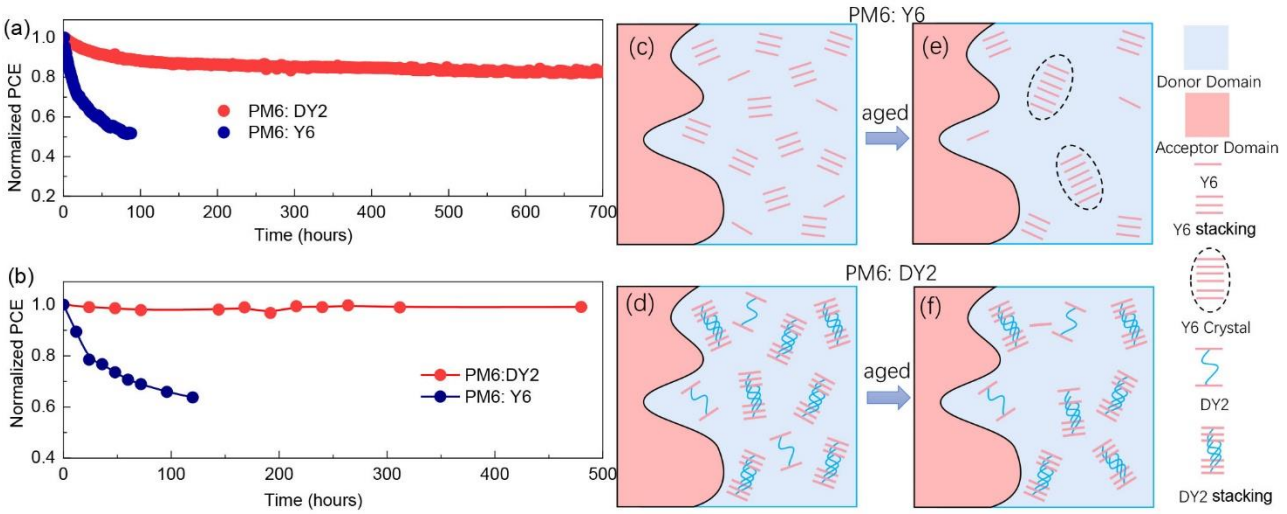

Figure 6. (a) MPP stability test of the PM6:**Y6** and PM6: **DY2** based devices under the illumination of a 100 mW cm^{-2} white LED. (b) Normalized PCEs of the PM6: **Y6** and PM6: **DY2** based devices under long-term annealing at 100 °C in nitrogen-filled glovebox. Illustration of thermodynamic relaxation from a favorable kinetically trapped morphology of (c) PM6: **Y6** and (e) PM6: **DY2** blend films, along with corresponding aged morphology (e and f). For simplicity, the demixing and crystallization of the acceptors in donor-rich domain are highlighted, the behavior of which critically degrade the device.

We further calculated the Flory–Huggins interaction parameter (χ) using the measurement of the T_m depression of the acceptor component in their blend through DSC, with the details of the calculations provided in the supporting information (Figure S6).[54-55] In this way, the miscibility of different blends can be identified via their χ value.[27] It has been disclosed that the PM6:Y6 blend features a hypo-miscibility, typically below the percolation threshold.[30] This means that the morphologies of PM6: Y6 blend is neither thermodynamically or sufficiently kinetically stabilized against over-purification and possibly crystallization, particularly at elevated temperatures where diffusion proceeds more readily. According to the Ade-O'Connor-Ghasemi framework, for those record-holing A-DA'D-A type acceptors, the increase of the χ value in their polymer blends is beneficial to their device stability.[31] In our calculation, χ values of 1.10 for the PM6: **DY2** and 0.87 for PM6: Y6 blend are obtained (Table S3). The higher χ value for PM6: **DY2** blend suggests a more hypo-miscible system relative to that of PM6: Y6, thus the diffusion-enabled demixing of the morphology can be well suppressed in PM6: **DY2** blend, improving the thermodynamic stability of

devices.

Conclusions

To address the morphology stability of record-holding A-DA'D-A type acceptor-based PSCs, here we proposed a new approach of covalently tether Y6 acceptors. In the molecular fragment, the Y6-based SMAs are linked to a benzyl core with a tunable flexible spacer to regulate their aggregation and diffusion behavior, which is largely different to their individual Y6 counterpart. This approach leads to improved structural order for higher and more balanced charge transport, and an increased molecular size to suppress diffusion in blend films, resulting a dramatically increased efficiency and stability in devices. The Y6-based device delivers a PCE of 16.93% along with a V_{OC} of 0.844V. For the dimer-based devices, one obvious advantage is their higher V_{OC} value of ca. 0.87 eV, leading to a higher efficiency of 17.85% for **DY2**. Thus, the tethered dimer strategy represents one successful example to provide an increased V_{OC} and corresponding higher efficiency. Most importantly, the dimer-based device shows substantially less burn-in efficiency loss, retaining more than 80% of the initial PCE for **DY2** based device after operating at MPP under continuous illumination for 700 hours. These findings suggest that the tethered Y6 based blend is a more hypo-miscible system relative to that of PM6:Y6, with the diffusion-enabled demixing of the morphology being well suppressed, resulting in a thermodynamically more stable device. Considering that the photophysical properties of the tethered SMAs can be further tuned through molecular engineering on structure (such as the SMA units, the spacer as well as the core units and number of the SMA unit tethered), this design strategy give a new direction to the future design of photovoltaic acceptors to simultaneously enhance the device efficiency and thermodynamically stability.

References

[1] H. Chen, R. Zhang, X. Chen, G. Zeng, L. Kobera, S. Abbrent, B. Zhang, W. Chen, G. Xu, J. Oh, S.-H. Kang, S. Chen, C. Yang, J. Brus, J. Hou, F. Gao, Y. Li, Y. Li, *Nat. Energy* **2021**, 6, 1045.

[2] P. Cheng, G. Li, X. Zhan, Y. Yang, *Nat. Photon.* **2018**, 12, 131.

[3] Y. Lin, J. Wang, Z.-G. Zhang, H. Bai, Y. Li, D. Zhu, X. Zhan, *Adv. Mater.* **2015**, 27, 1170.

[4] Y. Liu, B. Li, C.-Q. Ma, F. Huang, G. Feng, H. Chen, J. Hou, L. Yan, Q. Wei, Q. Luo, Q. Bao, W. Ma, W. Liu, W. Li, X. Wan, X. Hu, Y. Han, Y. Li, Y. Zhou, Y. Zou, Y. Chen, Y. Li, Y. Chen, Z. Tang, Z. Hu, Z.-G. Zhang, Z. Bo, *Sci. China Chem* **2022**, 65, 224.

[5] L. Zuo, S. B. Jo, Y. Li, Y. Meng, R. J. Stoddard, Y. Liu, F. Lin, X. Shi, F. Liu, H. W. Hillhouse, D. S. Ginger, H. Chen, A. K. Y. Jen, *Nat. Nanotech.* **2022**, 17, 53.

[6] K. Chong, X. Xu, H. Meng, J. Xue, L. Yu, W. Ma, Q. Peng, *Adv. Mater.* **2022**, 34, 2109516.

[7] C. Li, J. Zhou, J. Song, J. Xu, H. Zhang, X. Zhang, J. Guo, L. Zhu, D. Wei, G. Han, J. Min, Y. Zhang, Z. Xie, Y. Yi, H. Yan, F. Gao, F. Liu, Y. Sun, *Nat. Energy* **2021**, 6, 605.

[8] G. Chai, Y. Chang, J. Zhang, X. Xu, L. Yu, X. Zou, X. Li, Y. Chen, S. Luo, B. Liu, F. Bai, Z. Luo, H. Yu, J. Liang, T. Liu, K. S. Wong, H. Zhou, Q. Peng, H. Yan, *Energy Environ. Sci.* **2021**, 14, 3469.

[9] S. Chen, L. Feng, T. Jia, J. Jing, Z. Hu, K. Zhang, F. Huang, *Sci. China Chem* **2021**, 64, 1192.

[10] X. Kong, J. Zhang, L. Meng, C. Sun, S. Qin, C. Zhu, J. Zhang, J. Li, Z. Wei, Y. Li, *CCS Chem* **2022**, DOI: 10.31635/ccschem.022.202202056.

[11] Y. Cui, Y. Xu, H. Yao, P. Bi, L. Hong, J. Zhang, Y. Zu, T. Zhang, J. Qin, J. Ren, Z. Chen, C. He, X. Hao, Z. Wei, J. Hou, *Adv. Mater.* **2021**, 33, 2102420.

[12] L. Zhu, M. Zhang, J. Xu, C. Li, J. Yan, G. Zhou, W. Zhong, T. Hao, J. Song, X. Xue, Z. Zhou, R. Zeng, H. Zhu, C.-C. Chen, R. C. I. MacKenzie, Y. Zou, J. Nelson, Y. Zhang, Y. Sun, F. Liu, *Nat. Mater.* **2022**, 21, 656.

[13] R. Ma, C. Yan, J. Yu, T. Liu, H. Liu, Y. Li, J. Chen, Z. Luo, B. Tang, X. Lu, G. Li, H. Yan, *ACS Energy Lett* **2022**, 2547.

[14] R. Sun, Y. Wu, X. Yang, Y. Gao, Z. Chen, K. Li, J. Qiao, T. Wang, J. Guo, C. Liu, X. Hao, H. Zhu, J. Min, *Adv. Mater.* **2022**, 34, 2110147.

[15] C. He, Y. Pan, Y. Ouyang, Q. Shen, Y. Gao, K. Yan, J. Fang, Y. Chen, C.-Q. Ma, J. Min, C. Zhang, L. Zuo, H. Chen, *Energy Environ. Sci.* **2022**, 15, 2537.

[16] Y. Wang, J. Lee, X. Hou, C. Labanti, J. Yan, E. Mazzolini, A. Parhar, J. Nelson, J.-S. Kim, Z. Li, *Adv. Energ. Mater.* **2021**, 11, 2003002.

[17] X. Du, T. Heumueller, W. Gruber, O. Almora, A. Classen, J. Qu, F. He, T. Unruh, N. Li, C. J. Brabec, *Adv. Mater.* **2020**, 32, 1908305.

[18] S. Park, T. Kim, S. Yoon, C. W. Koh, H. Y. Woo, H. J. Son, *Adv. Mater.* **2020**, 32, 2002217.

[19] A. J. Clarke, J. Luke, R. Meitzner, J. Wu, Y. Wang, H. K. H. Lee, E. M. Speller, H. Bristow, H. Cha, M. J. Newman, K. Hooper, A. Evans, F. Gao, H. Hoppe, I. McCulloch, U. S. Schubert, T. M. Watson, J. R. Durrant, W. C. Tsoi, J.-S. Kim, Z. Li, *Cell. Rep. Phys. Sci.* **2021**, 2, 100498.

[20] Q. Burlingame, X. Huang, X. Liu, C. Jeong, C. Coburn, S. R. Forrest, *Nature* **2019**, 573, 394.

[21] G. Yu, J. Gao, J. C. Hummelen, F. Wudl, A. J. Heeger, *Science* **1995**, 270, 1789.

[22] Z. Wang, K. Gao, Y. Kan, M. Zhang, C. Qiu, L. Zhu, Z. Zhao, X. Peng, W. Feng, Z. Qian, X. Gu, A. K. Y. Jen, B. Z. Tang, Y. Cao, Y. Zhang, F. Liu, *Nat. Commun.* **2021**, 12, 332.

[23] J. Yuan, Y. Zhang, L. Zhou, G. Zhang, H.-L. Yip, T.-K. Lau, X. Lu, C. Zhu, H. Peng, P. A. Johnson, M. Leclerc, Y. Cao, J. Ulanski, Y. Li, Y. Zou, *Joule* **2019**, 3, 1140.

[24] J. Yuan, T. Huang, P. Cheng, Y. Zou, H. Zhang, J. L. Yang, S.-Y. Chang, Z. Zhang, W. Huang, R. Wang, D. Meng, F. Gao, Y. Yang, *Nat. Commun.* **2019**, 10, 570.

[25] K. Jiang, Q. Wei, J. Y. L. Lai, Z. Peng, H. K. Kim, J. Yuan, L. Ye, H. Ade, Y. Zou, H. Yan, *Joule* **2019**, 3, 3020.
[26] H. Cha, J. Wu, A. Wadsworth, J. Nagitta, S. Limbu, S. Pont, Z. Li, J. Searle, M. F. Wyatt, D. Baran, J.-S. Kim, I. McCulloch, J. R. Durrant, *Adv. Mater.* **2017**, 29, 1701156.
[27] L. Ye, B. A. Collins, X. Jiao, J. Zhao, H. Yan, H. Ade, *Adv. Energ. Mater.* **2018**, 8, 1703058, 1703058.
[28] N. Li, J. D. Perea, T. Kassar, M. Richter, T. Heumueller, G. J. Matt, Y. Hou, N. S. Güldal, H. Chen, S. Chen, S. Langner, M. Berlinghof, T. Unruh, C. J. Brabec, *Nat. Commun.* **2017**, 8, 14541.
[29] M. Ghasemi, H. Hu, Z. Peng, J. J. Rech, I. Angunawela, J. H. Carpenter, S. J. Stuard, A. Wadsworth, I. McCulloch, W. You, H. Ade, *Joule* **2019**, 3, 1328.
[30] Y. Qin, N. Balar, Z. Peng, A. Gadisa, I. Angunawela, A. Bagui, S. Kashani, J. Hou, H. Ade, *Joule* **2021**, 5, 2129.
[31] M. Ghasemi, N. Balar, Z. Peng, H. Hu, Y. Qin, T. Kim, J. J. Rech, M. Bidwell, W. Mask, I. McCulloch, W. You, A. Amassian, C. Risko, B. T. O'Connor, H. Ade, *Nat. Mater.* **2021**, 20, 525.
[32] G. Wang, F. S. Melkonyan, A. Facchetti, T. J. Marks, *Angew. Chem. Int. Ed.* **2019**, 58, 4129.
[33] H. Kang, W. Lee, J. Oh, T. Kim, C. Lee, B. J. Kim, *Acc. Chem. Res.* **2016**, 49, 2424.
[34] J. Wang, Y. Cui, Y. Xu, K. Xian, P. Bi, Z. Chen, K. Zhou, L. Ma, T. Zhang, Y. Yang, Y. Zu, H. Yao, X. Hao, L. Ye, J. Hou, *Adv. Mater.* **2022**, 34, 2205009.
[35] Z.-G. Zhang, Y. Li, *Angew. Chem. Int. Ed.* **2021**, 60, 4422.
[36] F. Lin, K. Jiang, W. Kaminsky, Z. Zhu, A. K. Y. Jen, *J. Am. Chem. Soc.* **2020**, 142, 15246.
[37] W. Wang, Q. Wu, R. Sun, J. Guo, Y. Wu, M. Shi, W. Yang, H. Li, J. Min, *Joule* **2020**, 4, 1070.
[38] H. Yu, Y. Wang, H. K. Kim, X. Wu, Y. Li, Z. Yao, M. Pan, X. Zou, J. Zhang, S. Chen, D. Zhao, F. Huang, X. Lu, Z. Zhu, H. Yan, *Adv. Mater.* **2022**, 34, 2200361.
[39] J. Yuan, H. Zhang, R. Zhang, Y. Wang, J. Hou, M. Leclerc, X. Zhan, F. Huang, F. Gao, Y. Zou, Y. Li, *Chem* **2020**, 6, 2147.
[40] H. Wang, C. Cao, H. Chen, H. Lai, C. Ke, Y. Zhu, H. Li, F. He, *Angew. Chem. Int. Ed.* **2022**, 61, e202201844.
[41] L. Zhang, Z. Zhang, D. Deng, H. Zhou, J. Zhang, Z. Wei, *Adv. Sci.* **2022**, 9, 2202513.
[42] W. Liu, J. Yuan, C. Zhu, Q. Wei, S. Liang, H. Zhang, G. Zheng, Y. Hu, L. Meng, F. Gao, Y. Li, Y. Zou, *Sci. China Chem* **2022**, 65, 1374.
[43] G. Han, Y. Yi, *Acc. Chem. Res.* **2022**, 55, 869.
[44] H. Fu, J. Yao, M. Zhang, L. Xue, Q. Zhou, S. Li, M. Lei, L. Meng, Z.-G. Zhang, Y. Li, *Nat. Commun.* **2022**, 13, 3687.
[45] S. M. Menke, N. A. Ran, G. C. Bazan, R. H. Friend, *Joule* **2018**, 2, 25.
[46] Y. Wang, D. Qian, Y. Cui, H. Zhang, J. Hou, K. Vandewal, T. Kirchartz, F. Gao, *Adv. Energy Mater.* **2018**, 8, 1801352.
[47] Z. Peng, L. Ye, H. Ade, *Mater. Horiz.* **2022**, 9, 577.
[48] J. Rivnay, S. C. B. Mannsfeld, C. E. Miller, A. Salleo, M. F. Toney, *Chem. Rev.* **2012**, 112, 5488.
[49] B. W. Boudouris, V. Ho, L. H. Jimison, M. F. Toney, A. Salleo, R. A. Segalman, *Macromolecules* **2011**, 44, 6653.
[50] S. R. Cowan, A. Roy, A. J. Heeger, *Phys. Rev. B* **2010**, 82.
[51] A. K. Kyaw, D. H. Wang, V. Gupta, W. L. Leong, L. Ke, G. C. Bazan, A. J. Heeger, *ACS Nano* **2013**, 7, 4569.
[52] P. Schilinsky, C. Waldauf, C. J. Brabec, *Appl. Phys. Lett.* **2002**, 81, 3885.
[53] M. Shi, T. Wang, Y. Wu, R. Sun, W. Wang, J. Guo, Q. Wu, W. Yang, J. Min, *Adv. Energ. Mater.* **2021**, 11, 2002709.
[54] T. Nishi, T. T. Wang, *Macromolecules* **1975**, 8, 909.
[55] C. Zhang, A. Mumyatov, S. Langner, J. D. Perea, T. Kassar, J. Min, L. Ke, H. Chen, K. L. Gerasimov, D. V. Anokhin, D. A. Ivanov, T. Ameri, A. Osvet, D. K. Susarova, T. Unruh, N. Li, P. Troshin, C. J. Brabec, *Adv. Energ. Mater.* **2017**, 7, 1601204.

Notes

The authors declare no competing financial interest.

Acknowledgements

S. L. R. Z. and M. Z. contributed equally to this work. The work was supported by the National Natural Science Foundation of China (Nos. 21734008 and 22175014), Fundamental Research Funds for the Central Universities (buctrc201822). Q.J. Zhou thanks the NanHu Young Scholar Supporting Program of XYNU. The authors thank the staff of the BL11 NCD-SWEET beamline at ALBA Synchrotron for their assistance in recording the GIWAXS data. The revised 2D GIWAXS data were acquired at beamline 7.3.3 while the RSoXS data were acquired at beamline 11.0.1.2 at the Advanced Light Source, LBNL, which is supposed by the Director, Office of Science, Office of Basic Energy Sciences, of the US Department of Energy under Contract No. DE-AC02-05CH11231. R. Z. thanks Prof. Chenhui Zhu for the GIWAXS measurement and Pro. Cheng Wang for the RSoXS measurement. J.A.S. acknowledges financial support from the Research Foundation - Flanders (FWO: grants 12Y7221N and V400622N) and M.B.J.R. acknowledges support from the KU Leuven Research Fund (C14/19/079, iBOF-21-085 PERSIST), and the KU Leuven Industrial Research Fund (C3/19/046). This research was also funded by Princess Nourah bint Abdulrahman University Researchers Supporting project number (PNURSP2022R1).

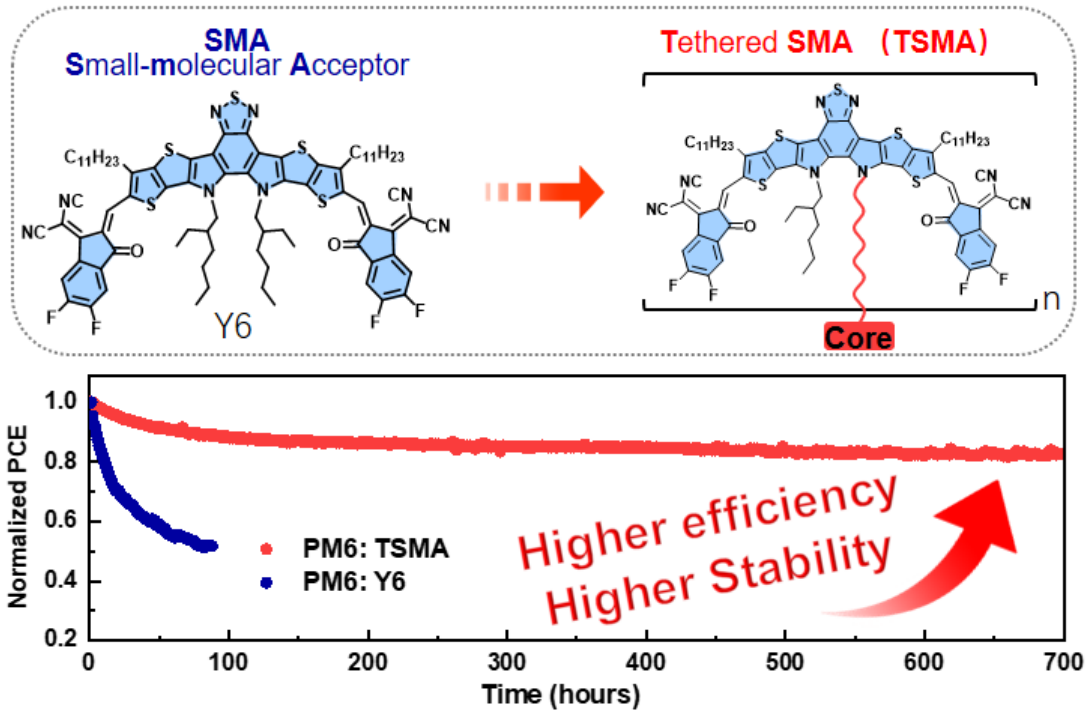

The thermodynamic relaxation of small-molecule acceptor (SMA) in its blend with polymer donor raises concerns related to the long-term operational stability of Polymer solar cells. With flexible spacers to restrict the motion of individual SMAs, the tethered SMAs show large glass transition temperatures to suppress the thermodynamic relaxation in mixed domains.